Journal of Geophysical Research - Oceans

Supporting Information for

$\Delta O_2/N_2$' as a Tracer of Mixed Layer Net Community Production: Theoretical Considerations and Proof-of-Concept

Robert W. Izett[1] & Philippe D. Tortell[1,2]

[1.] Department of Earth, Ocean and Atmospheric Sciences, University of British Columbia, Vancouver, BC, Canada.

[2.] Botany Department, University of British Columbia, Vancouver, BC, Canada.

Contents of this file

Introduction

This supporting information provides supplementary figures, tables and explanations for the interpretation of the main text. Additional formulae derivations (S1) and error analyses (S2, Table S2) are also presented. A more detailed description of field applications of the N_2' approach presented in the main text is provided in section S3, with accompanying Matlab code and examples in a toolbox repository (available at *https://doi.org/10.5281/zenodo.4024952*, with link to *github.com/rizett/O2N2_NCP_toolbox* repository). Matlab code and output from the 1D numerical simulations described in the main text are also provided at the same repository.

S1. One-dimensional mixed layer physical gas model

As per Eq. 2 in the main text, we applied the following mixed layer budget to O_2, Ar and N_2:

$$MLD \cdot \frac{dC}{dt} = F_d + F_B + F_M. \quad \text{(S1.1)}$$

In this equation, MLD is the mixed layer depth (m), dC/dt represents the change in gas concentration over time resulting from physical processes, F_d represents the diffusive air-sea exchange flux, F_B is the combined small and large bubble fluxes (representing air-sea exchange processes via complete bubble injection, F_C, or partial exchange, F_P, respectively), and F_M is the sum of vertical diapycnal mixing (F_k), upwelling (F_w) and entrainment during mixed layer deepening (F_e). We used the model of Liang et al. (2013) to parameterize the air-sea exchange terms (F_d, F_c and F_p) in ice-free waters, and the model of Butterworth & Miller (2016) (which excludes explicit bubble fluxes) in partially-ice covered waters. We estimated the vertical mixing terms from subsurface gas concentrations (C_{deep}) and mixing rates as described in the main text. Equation S1.1 can be expanded as:

$$MLD \cdot \frac{dC}{dt} = F_d + F_C + F_P + F_k + F_w + F_e. \quad \text{(S1.2)}$$

$$MLD \cdot \frac{dC}{dt} = \left[k_d \left(C_{eq} \cdot \frac{SLP}{1\ atm} - C\right)\right] + \left[\beta \cdot k_p \left(C_{eq} \cdot (1 + \Delta P) \cdot \frac{SLP}{1\ atm} - C\right) + \beta \cdot F_c\right] + \left[\kappa_Z \cdot \frac{dC}{dz}\right] + \left[\omega \cdot \frac{dC}{dz} \cdot MLD\right] + \left[\frac{dMLD}{dt} \cdot \left(C_{deep} - C\right)\right] \quad \text{(S1.3)}$$

where k_d and k_p are the diffusive and bubble-mediated air-sea exchange coefficients, ΔP is the supersaturation increase caused by partially-dissolving bubbles, and F_C is the small bubble flux, all parameterized in Liang et al. (2013) and Butterworth & Miller (2016) (F_p and F_C are zero in ice-covered conditions). Sensitivity analyses comparing our simulation results with in-situ observations at Ocean Station Papa suggest that a bubble-mediated gas flux scaling coefficient, β, of 0.5 is appropriate, as in Yang et al. (2017) (see Fig. 5 in the main text). C_{eq} (mmol m^{-3}) is the gas solubility at equilibrium, per Garcia & Gordon (1993) for O_2 and Hamme & Emerson (2004) for Ar and N_2. SLP represents the sea level pressure (atm). The mixing terms are represented by the eddy diffusivity coefficient (κ_Z; $m^2\ d^{-1}$), advection velocity (ω, proportional to wind speed; m d^{-1}), the rate of mixed layer deepening (dMLD/dt; m d^{-1}), the surface-to-subsurface gas gradient (dC/dZ = (C_{deep} – C)/dZ; mmol m^{-4}) and the deep gas concentration (C_{deep}; mmol m^{-3}). We set Ar_{deep} and $N_{2,deep}$ values by adjusting subsurface ΔAr and $\Delta N_2/Ar$ (i.e. $\Delta N_2/Ar_{deep}$), while holding $O_{2,deep}$ constant at equilibrium concentrations (experimental simulations) or set to values based on observations (realistic simulations). The entrainment term is zero when the mixed layer shoals, and all mixing terms were set to zero in run a (no mixing) of the experimental and realistic simulations.

Matlab code for performing simulations with our 1D gas model is provided in the O2N2_NCP_toolbox on *Zenodo* (*https://doi.org/10.5281/zenodo.4024952*) and *GitHub* (*github.com/rizett/O2N2_NCP_toolbox*). Users can define forcing input (e.g. environmental data, initial conditions, and mixing coefficients) and experimental settings (e.g. see details in table 1 in the main text), and can specify the air-sea flux parameterization.

S1.2 N_2' budget: Quasi-steady-state conditions and estimating O_2 re-equilibration timescale

The N_2' term is derived by predicting N_2 and Ar divergence over a MLD O_2 re-equilibration time scale (defined below in Eq. S6.3), and subtracting this value from observed N_2 saturation. To derive N_2', we simplified the MLD budget described in Eq. S1 by combining all mixing processes into a single term. We set F_e to zero, and collapsed the remaining fluxes with a single coefficient, κ (κ = κ_Z + ω*dz; m^2 d^{-1}):

$$F_k + F_w + F_e \approx \frac{dC}{dZ}\kappa \quad \text{(S2)}$$

Combining Eqs. S1.2 and S2 yields the simplified budget used to perform N_2' calculations (Eq. 3 in the main text), which was evaluated over one O_2 re-equilibration time, τ_{O2} (Eq. S6.3), prior to observations (Fig. S2).

$$MLD \cdot \frac{dC}{dt} = \left[k_d\left(C_{eq} \cdot \frac{SLP}{1\ atm} - C\right)\right] + \left[\beta \cdot k_p\left(C_{eq} \cdot (1 + \Delta P) \cdot \frac{SLP}{1\ atm} - C\right) + \beta \cdot F_c\right] + \frac{dC}{dZ}\kappa \quad \text{(S3)}$$

Using this budget, we calculated the expected divergence between Ar and N_2 saturation states at the end of the τ_{O2} time period, and subtracted this difference from the true ΔN_2 (Eq. 4 in the main text; Fig. S2). In the model setting, true ΔN_2 (i.e. ΔN_2^{true}) is the N_2 supersaturation anomaly predicted by the full MLD budget (Eq. S1), and in field studies, ΔN_2^{true} is the measured N_2 supersaturation. Figure S2 shows a representation of calculations performed with the full and condensed N_2' MLD budgets. The approach to estimating N_2' was repeated for all time points in the full model simulations. In field studies, calculations will be performed over the O_2 re-equilibration timeframe prior to each observation, in an analogous approach to calculations of a weighted piston velocity (Reuer et al., 2007). Matlab code, and example data are provided at *https://doi.org/10.5281/zenodo.4024952*. Refer to section S3 for further details.

The analytical solution to Eq. S3 describes the quasi-steady-state gas condition, and can be derived by further simplifying the gas budget to combine the air-sea exchange terms, following (Woolf, 1997) and Eq. 2 in Liang et al. (2013):

$$F_d + F_C + F_P \approx -k_T\left(C - C_{eq}\left(1 + \Delta_{eq}\right)\frac{SLP}{1\ atm}\right) \quad \text{(S4)}$$

Here k_T is the pooled diffusive and bubble-mediated gas transfer coefficients (i.e. $k_d + \beta \cdot k_P$) and Δ_{eq} is the bubble-induced steady-state gas supersaturation. This approximation simplifies the derivation of the analytical solution, and matches the net air-sea flux predicted by the full parameterization (as in Eq. S1) with a relative accuracy of ~2 % over a range of wind speeds (0-25 m s^{-1}) and gas saturation states (90-110 %; results not shown). The analytical solution can subsequently be derived by discretizing the simplified gas budget into sufficiently short time

increments, dt, so that MLD, k_T, Δ_{eq}, C_{deep} and κ can be considered constant. Below, we derive the analytical solution to the simplified budget through the following steps:

1) Expand Eq. S3 with simplified gas flux terms.

$$\frac{dC}{dt} = \frac{-k_T}{MLD}\left(C - C_{eq}\left(1 + \Delta_{eq}\right)\frac{SLP}{1\ atm}\right) + \frac{C_{deep} - C}{dZ}\frac{\kappa}{MLD} \quad \text{(S5.1)}$$

2) Simplify k_T/MLD and κ/(dZ · MLD) as K_1 and K_2, respectively, and re-write the equation by combining terms.

$$\frac{dC}{dt} = -(K_1 + K_2) \cdot C + K_1 \cdot C_{eq} \cdot \left(1 + \Delta_{eq}\right)\frac{SLP}{1\ atm} + K_2 \cdot C_{deep} \quad \text{(S5.2)}$$

3) Further simplify by expressing (K_1 + K_2) as P, $\left(K_1 \cdot C_{eq} \cdot \left(1 + \Delta_{eq}\right) \cdot \frac{SLP}{1\ atm} + K_2 \cdot C_{deep}\right)$ as Q, and dC/dt as C'. Apply an integration factor of e^{Pt}.

$$C' = -\mathrm{P} \cdot C + Q \quad \text{(S5.3)}$$

$$C' \cdot e^{Pt} + \mathrm{P} \cdot C \cdot e^{Pt} = Q \cdot e^{Pt} \quad \text{(S5.4)}$$

4) Note that d/dt($C \cdot e^{Pt}$) = $C' \cdot e^{Pt} + \mathrm{P} \cdot C \cdot e^{Pt}$ by the product rule.

$$\frac{d}{dt}(C \cdot e^{Pt}) = Q \cdot e^{Pt} \quad \text{(S5.5)}$$

$$C \cdot e^{Pt} = Q \cdot \int e^{Pt}\, dt \quad \text{(S5.6)}$$

5) Since P and Q (defined above in step 3) are considered constant over dt, Eq. S5.6 can be integrated simply. In Eq. S5.7, R is the integration constant.

$$C = \frac{Q}{P} + R \cdot e^{-Pt} \quad \text{(S5.7)}$$

6) Finally, by setting C(t=0) to be the initial condition, C_0, we derive a single analytical solution, by re-substituting the simplifying terms (P and Q defined above in step 3) for the gas flux terms.

$$R = C_0 - \frac{Q}{P} \quad \text{(S5.8)}$$

$$C = \frac{k_T \cdot C_{eq} \cdot \left(1 + \Delta_{eq}\right) \cdot \frac{SLP}{1\ atm} + \frac{\kappa}{\mathrm{dz}} \cdot C_{deep}}{k_T + \frac{\kappa}{\mathrm{dz}}} + \left(C_0 - \frac{k_T \cdot C_{eq} \cdot \left(1 + \Delta_{eq}\right) \cdot \frac{SLP}{1\ atm} + \frac{\kappa}{\mathrm{dz}} \cdot C_{deep}}{k_T + \frac{\kappa}{\mathrm{dz}}}\right) \cdot e^{-\left(\frac{k_T}{MLD} + \frac{\kappa}{\mathrm{dz} \cdot \mathrm{MLD}}\right)t} \quad \text{(S5.9)}$$

When mixing is negligible (i.e. κ ≈0 $m^2\ d^{-1}$), Eq. S5.9 simplifies to

$$C = C_{eq} \cdot \left(1 + \Delta_{eq}\right) \cdot \frac{SLP}{1\ atm} + \left(C_0 - C_{eq} \cdot \left(1 + \Delta_{eq}\right) \cdot \frac{SLP}{1\ atm}\right) \cdot e^{-\left(\frac{k_T}{MLD}\right)t} \quad \text{(S5.10)}$$

The analytical solution is useful for understanding quasi-steady-state gas conditions, and the rate of response to perturbations. For example, the quasi-steady-state gas concentration, C_{SS}, can be predicted from Eq. S5.9 as t approaches infinity, and C approaches the value of the first term:

$$C_{SS} = \frac{k_T \cdot C_{eq} \cdot \left(1+\Delta_{eq}\right) \cdot \frac{SLP}{1\ atm} + \frac{\kappa}{\mathrm{dz}} \cdot C_{deep}}{k_T + \frac{\kappa}{\mathrm{dz}}} \quad \text{(S5.11)}$$

Subsequently, the mixed layer O_2 re-equilibration timescale, τ_{O2}, can be estimated as the time required for air-sea gas exchange and vertical mixing processes to re-establish the quasi-steady-state condition. We thus estimated τ_{O2} by setting $(C - C_{SS}) / (C_0 - C_{SS})$ to be 0.01 (i.e. $C - C_{SS} << C_0 - C_{SS}$) and t to τ_{O2}:

$$C = C_{SS} + (C_0 - C_{SS}) \cdot e^{-\left(\frac{k_T}{MLD} + \frac{\kappa}{\mathrm{dz} \cdot \mathrm{MLD}}\right)\tau_{O2}} \quad \text{(S6.1)}$$

$$\frac{C - C_{SS}}{C_0 - C_{SS}} = 0.01 = e^{-\left(\frac{k_T}{MLD} + \frac{\kappa}{\mathrm{dz} \cdot \mathrm{MLD}}\right)\tau_{O2}} \quad \text{(S6.2)}$$

$$\tau_{O2} = \frac{-\ln(0.01) \cdot \mathrm{MLD}}{\left(k_T + \frac{\kappa}{\mathrm{dz}}\right)} \quad \text{(S6.3)}$$

The MLD O_2 re-equilibration time calculated by this approach represents several MLD O_2 residence times, which is typically approximated by MLD/k_T.

Since the exponential weighting function used to calculate O_2 piston velocities is typically negligible after ~30 days (Teeter et al., 2018), calculation of gas transfer coefficients (i.e. Eq. 5 in the main text) will not be significantly impacted by the choice to weight k_{O2} over τ_{O2} or MLD/k_T. However, calculating τ_{O2} by this approach reflects the contribution of vertical mixing (proportional to κ) in reducing O_2 cycling in surface waters, and more fully represents the timeframe of gas re-equilibration within the MLD. This timescale, τ_{O2}, is therefore more appropriate for N_2' calculations relevant to NCP derivation. Indeed, when the N_2' calculations are performed over a timescale represented by MLD/k_T, differences between Ar and N_2 relevant to NCP calculations are not fully reconciled (Fig. S2b). In ocean environments, where MLD, k_T and κ vary in time, τ_{O2} should be estimated using 30- to 60-day weighted values for these terms, where possible, or from ship-based observations.

S2. Uncertainty analyses

S2.1 ΔN_2' parameter uncertainty

We performed a Monte Carlo analysis on the real-OSP and real-BB full mixing (run c) simulations to determine the contributions of individual and combined parameterization uncertainty to errors in $\Delta O_2/N_2$'. This analysis was conducted by randomly varying each of the input variables (wind speed, SST, SLP, MLD), air-sea flux (F_d, F_P, F_C, β) and mixing terms (κ, $\Delta N_2/Ar_{deep}$) in the N_2' MLD budget (Eq. S4 above, and Eq. 3 in the main text) around their estimated uncertainties (Table S1), and performing 100 (for individual parameter errors) or 1000 (for combined errors) iterations of N_2' calculations.

We used uncertainties of ± 2.5 m s^{-1}, ± 0.75 ºC and ± 2 mbar in the wind speed, SST and SLP data based on a comparison of in-situ observations (from ships, moorings and weather buoys) with various gridded products. For observations based in the Subarctic NE Pacific, the Cross-Calibrated Multi-Parameter (CCMP) wind speed product (provided by Remote Sensing Systems at *www.remss.com*; Atlas et al., 2011), NOAA High Resolution SST Dataset (provided by NOAA ESRL at https://psl.noaa.gov/; Reynolds et al., 2007), and NCEP/NCAR reanalysis 2 SLP (provided by NOAA ESRL at psl.noaa.gov; Kalnay et al., 1996) products compared best with observations from moorings in coastal and off-shore waters. In the Arctic, the NCEP/NCAR Reanalysis 2 wind product performed best.

The air-sea flux terms (F_d, F_P and F_C) depend on the choice of gas transfer parameterization. In the present study, we use the bubble-mediated model of Liang et al. (2013), as it was parameterized for O_2 and N_2, and is considered valid for gases with similarly low solubility. Over a range of wind speeds and temperatures, we estimate the relative uncertainty in these terms to be ~18-24 %, based on the standard deviation of values derived using several gas transfer parameterizations (Stanley et al., 2009; Sweeney et al., 2007; Vagle et al., 2010; Wanninkhof, 2014; Woolf, 1997). These errors are roughly consistent with Wanninkhof (2014), who estimated a mean total error in the air-sea gas flux of ~20 %. We therefore followed Bushinsky & Emerson (2015) by assigning a relative error of 15 % to F_d, F_P and F_C in our Monte Carlo analysis. Finally, we ascribed an error of ±5 m to estimates of the MLD, following Izett et al. (2018), an error of ±0.14 to β based on Emerson et al. (2019), and conservative uncertainties of ±10^{-5} m^2 s^{-1} and 0.25 % to

Overall, we find that uncertainty in the sea surface temperature product (mean 0.07 %) contributes the largest individual errors to $\Delta O_2/N_2$'. This is unsurprising as seasonal SST variability, which drives diffusive air-sea exchange, contributes to strong variability in $\Delta N_2/Ar$ (see main text). Errors in the mixing coefficient term were next greatest (mean 0.02 %), while errors in the bubble-flux terms (β, F_C, F_P) were generally small, due to the low prevalence of high wind speeds. Errors associated with these terms were typically larger during autumn to spring, when wind speeds were elevated. The combined uncertainty from all parameterizations is 0.09 %, on average, across both real-OSP and real-BB simulations.

S2.2 Assumption uncertainty

The N_2' approach assumes constant values of MLD, salinity, κ, and $\Delta N_2/Ar_{deep}$, based on the availability of data products and at-sea measurements (see main text for details). To evaluate the uncertainty in N_2' incurred by these assumptions, we compared calculations on the real-OSP and real-BB full mixing (run c) simulations in which these values were held constant against calculations in which they were allowed to vary, based on values in the full model simulations. Across both simulations, we found mean errors in $\Delta O_2/N_2$' from these assumptions of 0.07 %

(range ~0.001 – 0.3; Table S1). This value is similar to the combined parameterization uncertainty, but can only be reduced through accurate estimation of the time-history of MLD, salinity κ, and $\Delta N_2/Ar_{deep}$ terms. This may not be feasible for many field measurement programs.

In general, the uncertainties associated with the N_2' assumptions were larger in the real-BB simulation (Fig. s9b) due to significant and rapid variability in subsurface temperature, and therefore subsurface N_2 and Ar concentrations, invoked in our model. These uncertainties, and the remaining biases in $\Delta N_2'/Ar$ ($\Delta O_2/Ar - \Delta O_2/N_2'$ almost as large as $\Delta O_2/Ar - \Delta O_2/N_2$ in Fig. s9b), are likely represent the upper range errors in the approach presented here, as subsurface inert gas concentrations likely do not vary as much in reality as they do in our modeled environment. In the absence of time-series observations of subsurface gas concentrations in Baffin Bay, we necessarily set $N_{2,deep}$ and Ar_{deep} equivalent to their equilibrium concentrations at the time-variable temperature and salinity conditions of the deep box layer. The large amplitude in temperature variability in this deep box layer results from significant shoaling of the MLD as the model progresses into summer months, and contributed to significant variability in subsurface N_2 and Ar concentrations. As the N_2' approach assumes these values are constant over the duration of calculations, failure to represent this variability will result in large remaining biases in $\Delta N_2'/Ar$. If deep gas concentrations do not vary to such large degrees in reality, the errors in N_2' would be significantly smaller, as in the real-OSP simulation.

S2.3 Uncertainty from N_2-fixation

We estimated the potential uncertainty in N_2' and $\Delta O_2/N_2'$ due to N_2-fixation by applying constant rates of N_2 removal (see main text for details) in 1D model simulations without vertical mixing over a range of constant u_{10} and SST. We compared the steady-state ΔN_2 from these runs against values obtained with N_2-fixation rates of zero. For the upper range of N_2-fixation observed in the ocean, we calculate a maximum steady-state deviation of ~0.3 % at very low wind speeds, but values are always less than 0.05 % above wind speeds of 6 m s^{-1} (Fig. S8c). Applying a constant N_2-fixation rate equivalent to the global observed maximum (see main text) to the real-OSP full mixing run resulted in deviations of less than 0.05 % in N_2 saturation when compared against the run excluding N_2-fixation. We thus conclude that N_2-fixation will have a negligible effect on $\Delta O_2/N_2'$ calculations in most oceanic waters.

S2.4 Total uncertainty

Our error analyses produce a total average uncertainty in $\Delta O_2/N_2'$ of 0.01 % (range 0.04 – 0.3; Table 1) resulting from the parameterization and assumption errors. On average, this is smaller than the offset between $\Delta O_2/Ar$ and uncorrected $\Delta O_2/N_2$. The upper range of uncertainty in $\Delta O_2/N_2'$ (including potential contributions from N_2-fixation) is represented in Fig. S9, which presents $\Delta O_2/Ar - \Delta O_2/N_2'$ from the realistic OSP and BB simulations (full mixing scenario / run c only). Since the assumption errors contribute the largest proportion to total $\Delta N_2'$ uncertainty, the total error in $\Delta O_2/N_2'$ is smallest when these values are small during periods of reduced MLD, κ and $\Delta N_2/Ar_{deep}$ variability (see Figs. 3-4 in the main text). In field studies, the error approximated here and potential uncertainty from in-situ O_2 and N_2 measurement accuracy will contribute to total uncertainty in $\Delta O_2/N_2'$.

We exclude the RMSE derived from the N_2 validation against observations (0.9 %; see main text) from the total estimated N_2' uncertainty, as this likely over-estimates the relative differences between Ar and N_2.

S3 Application of the N_2' approach to field data

In field-based applications, derivation of N_2' estimates requires measurements of surface gas concentrations (N_2), hydrographic data (temperature and salinity) and best estimates of the MLD and the mixing terms κ and $\Delta N_2/Ar_{deep}$ at the time of sampling. MLD can be derived by interpolating between CTD casts or using climatological datasets, whereas mixing terms can be estimated from observations, numerical models or archived datasets (see main text for details). Information on ocean conditions (SST, u_{10}, and SLP) prior to gas measurements, during the O_2 re-equilibration time frame (typically ~60-90 days in ice-free waters; Eq. 6.3), are also necessary to perform calculations. These "historic" data can be obtained from reanalysis or satellite products. The MLD, κ and $\Delta N_2/Ar_{deep}$ will commonly be assumed constant backwards in time, based on values at the time of ship-board gas observation, or based on alternative sources (see main text).

In Eq. 4 in the main text, ΔN_2^{obs} is the measured gas supersaturation condition, and ΔN_2^{est} and ΔAr^{est} are predicted by the calculations described above in section S1.2. N_2' calculations are performed in a similar approach to piston velocity weighting (Reuer et al., 2007), and the weighting function (Eq. 4 in Teeter et al., 2018) should be applied to the historic estimates of wind speed and κ when evaluating the O_2 re-equilibration and N_2' timescale from Eq. 6.3. All input data should have the same spatial resolution as continuous O_2/N_2 observations, with N_2' calculations applied independently to each underway gas measurement.

In using our Matlab codes (with examples in the O2N2_NCP_toolbox; *https://doi.org/10.5281/zenodo.4024952*), users provide the historic datasets, observed ΔN_2, and specify the gas transfer parameterization (including β gas scaling term) best suited to their region of study. These codes can be used as templates for future studies, and can be modified to incorporate future developments. The main codes we provided were written by R. Izett, with additional scripts cited accordingly.

References

Atlas, R., Hoffman, R. N., Ardizzone, J., Leidner, S. M., Jusem, J. C., Smith, D. K., & Gombos, D. (2011). A cross-calibrated, multiplatform ocean surface wind velocity product for meteorological and oceanographic applications. *Bulletin of the American Meteorological Society*, *92*, 157–174. https://doi.org/10.1175/2010BAMS2946.1

Bushinsky, S. M., & Emerson, S. (2015). Marine biological production from in situ oxygen measurements on a profiling float in the subarctic Pacific Ocean. *Global Biogeochemical Cycles*, *29*, 2050–2060. https://doi.org/10.1002/2015GB005251

Butterworth, B. J., & Miller, S. D. (2016). Air-sea exchange of carbon dioxide in the Southern Ocean and Antarctic marginal ice zone. *Geophysical Research Letters*, *43*, 7223–7230. https://doi.org/10.1002/2016GL069581

Emerson, S., Yang, B., White, M., & Cronin, M. (2019). Air-Sea Gas Transfer: Determining Bubble Fluxes With In Situ N2 Observations. *Journal of Geophysical Research: Oceans*, *124*(4), 2716–2727. https://doi.org/10.1029/2018JC014786

Garcia, H. E., & Gordon, L. I. (1993). Erratum: Oxygen solubility in seawater: better fitting equations. *Limnology and Oceanography*, *38*, 656.

Hamme, R. C., & Emerson, S. R. (2004). The solubility of neon , nitrogen and argon in distilled water and seawater. *Deep-Sea Research Part I*, *51*, 1517–1528. https://doi.org/10.1016/j.dsr.2004.06.009

Izett, R., Manning, C. C., Hamme, R. C., & Tortell, P. D. (2018). Refined estimates of net community production in the Subarctic Northeast Pacific derived from ΔO2/Ar measurements with N2O-based corrections for vertical mixing. *Global Biogeochemical Cycles*, *32*, 326–350. https://doi.org/https://doi.org/10.1002/2017GB005792

Kalnay, E., Kanamitsu, M., Kistler, R., Collins, W., Deaven, D., Gandin, L., et al. (1996). The NCEP/NCAR 40-year reanalysis project. *Bulletin of the American Meteorological Society*, *77*, 437–471. https://doi.org/10.1175/1520-0477(1996)077<0437:TNYRP>2.0.CO;2

Liang, J.-H. H., Deutsch, C., McWilliams, J. C., Baschek, B., Sullivan, P. P., & Chiba, D. (2013). Parameterizing bubble-mediated air-sea gas exchange and its effect on ocean ventilation. *Global Biogeochemical Cycles*, *27*(3), 894–905. https://doi.org/10.1002/gbc.20080

Reuer, M. K., Barnett, B. A., Bender, M. L., Falkowski, P. G., & Hendricks, M. B. (2007). New estimates of Southern Ocean biological production rates from O_2/Ar ratios and the triple isotope composition of O_2. *Deep Sea Research I*, *54*(2007), 951–974. https://doi.org/10.1016/j.dsr.2007.02.007

Reynolds, R. W., Smith, T. M., Liu, C., Chelton, D. B., Casey, K. S., & Schlax, M. G. (2007). Daily High-Resolution-Blended Analyses for Sea Surface Temperature. *Journal of Climate*, *20*, 5473-5496.

Stanley, R. H. R., Jenkins, W. J., Lott, D. E., & Doney, S. C. (2009). Noble gas constraints on air-sea gas exchange and bubble fluxes. *Journal of Geophysical Research: Oceans*, *114*(11), 1–14. https://doi.org/10.1029/2009JC005396

Sweeney, C., Gloor, E., Jacobson, A. R., Key, R. M., McKinley, G., Sarmiento, J. L., & Wanninkhof, R. (2007). Constraining global air–sea gas exchange for CO2 with recent bomb 14C measurements. *Global Biogeochemical Cycles*, *21*(GB2015). https://doi.org/doi:10.1029/2006GB002784

Teeter, L., Hamme, R. C., Ianson, D., & Bianucci, L. (2018). Accurate Estimation of Net Community Production From O2/Ar Measurements. *Global Biogeochemical Cycles*, 1–19. https://doi.org/10.1029/2017GB005874

Vagle, S., McNeil, C., & Steiner, N. (2010). Upper ocean bubble measurements from the NE Pacific and estimates of their role in air-sea gas transfer of the weakly soluble gases nitrogen and oxygen, *115*, C12054. https://doi.org/10.1029/2009JC005990

Wang, S., Kranz, S. A., Kelly, T. B., Song, H., Stukel, M. R., & Cassar, N. (2020). Lagrangian Studies of Net Community Production: The Effect of Diel and Multiday Nonsteady State Factors and Vertical Fluxes on O 2 /Ar in a Dynamic Upwelling Region. *Journal of Geophysical Research: Biogeosciences*, *125*(6), 1–19. https://doi.org/10.1029/2019jg005569

Wanninkhof, R. (2014). Relationship between wind speed and gas exchange over the ocean revisited. *Limnology and Oceanography: Methods*, *12*(6), 351–362. https://doi.org/10.1029/92JC00188

Woolf, D. K. (1997). *Bubbles and their role in gas exchange*. *The Sea Surface and Global Change*. https://doi.org/10.1017/cbo9780511525025.007

Yang, B., Emerson, S. R., & Bushinsky, S. M. (2017). Annual net community production in the subtropical Pacific Ocean from in-situ oxygen measurements on profiling floats. *Global Biogeochemical Cycles*, *31*, 728–744. https://doi.org/10.1002/2016GB005545

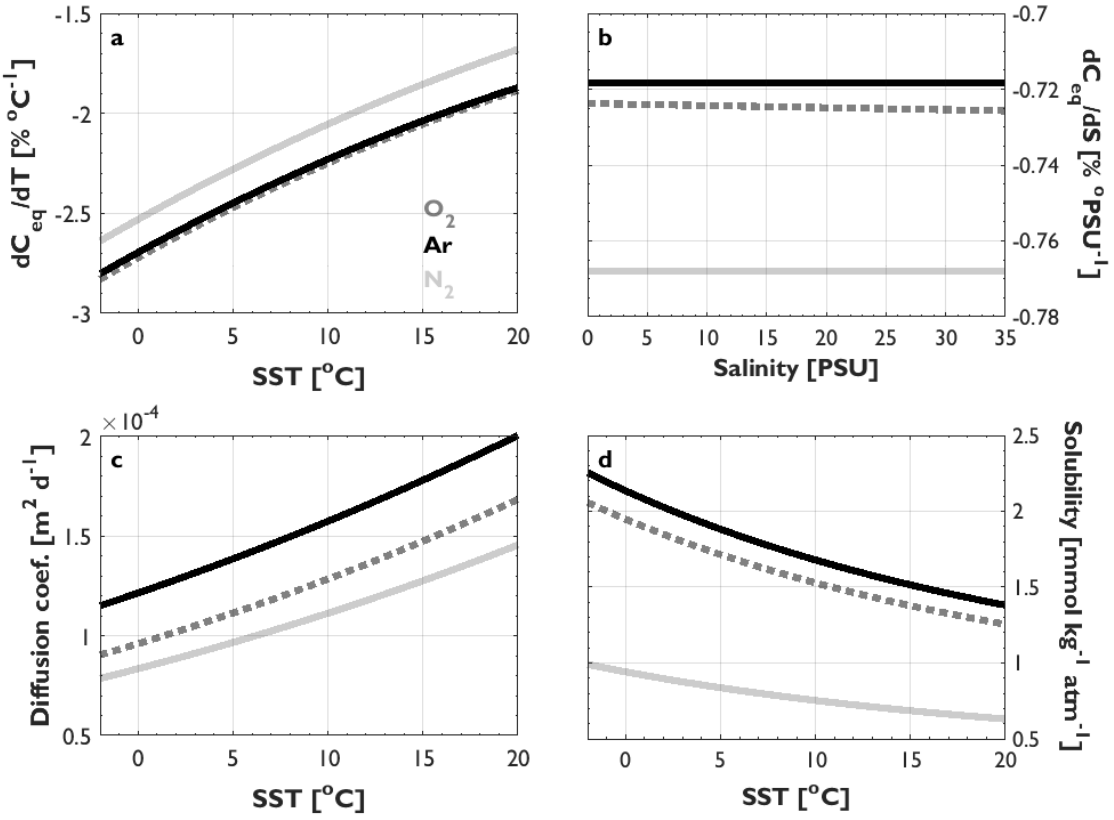

Figure S1. The differential physical properties of O_2 (dotted grey), Ar (black) and N_2 (solid grey) across a range of temperatures and salinities. Panels (a) and (b) represent the solubility-temperature and -salinity dependence of each gas, respectively, panel (c) presents their air-sea diffusion exchange coefficients, and panel (d) shows the Henry's Law solubility for each gas in one standard atmosphere of dry air. Lines represent average values over a salinity range of 0-35 PSU (panels a, c and d) or a temperature range of -2 to 10 °C (panel b).

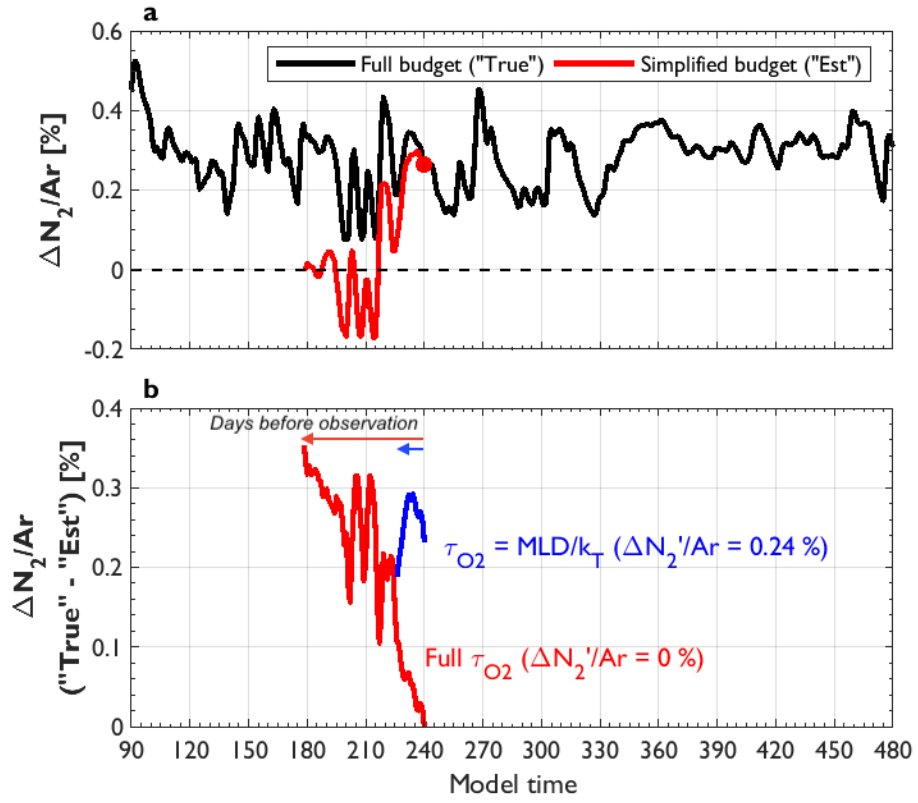

Figure S2. An example of the application of the N_2' approach. Panel (a) shows $\Delta N_2/Ar$ predicted in a full model simulation (i.e. based on ΔN_2^{true} and ΔAr from a real-OSP simulation with mixing; black line), and one example of values calculated using ΔN_2^{est} and ΔAr^{est} (red line, Eq. 4 in the main text) derived by evaluating the N_2' budget over the O_2 re-equilibration timescale, τ_{O2} before the time of observation (Eq. 3 in the main text and Eq. S3 above). ΔN_2' was estimated by subtracting the estimated difference between ΔN_2 and ΔAr (i.e. $\Delta N_2^{est} - \Delta Ar^{est}$) obtained from the simplified model from ΔN_2^{true} at the time marked by the red dot. This was repeated for all time points obtained from the full model simulation. Panel (b) represents the difference in $\Delta N_2/Ar$ predicted by the full model and the simplified model over the time frame of calculations. Two sets of calculations are shown: one for the full τ_{O2} (estimated from Eq. S6.3) and one set performed over an O_2 residence time, approximated as MLD/k_{O2}. Note that the latter is too short of a time period to fully-reconcile ΔN_2 and ΔAr differences relevant to NCP calculations.

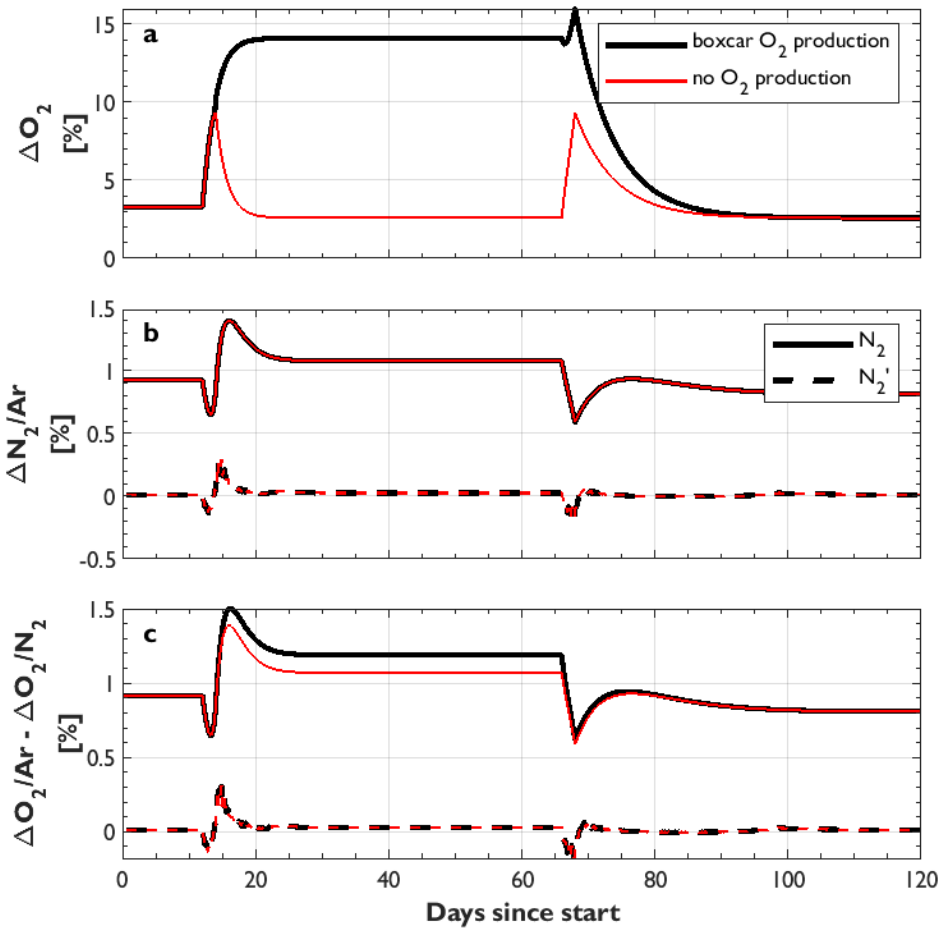

Figure S3. Results from a numerical simulation (Ex-IF 3) exploring the impact of biological O_2 production on surface gas concentrations. Black and red lines represent simulation results obtained with (black) and without (red) biological O_2 production (20 mmol O_2 m^{-2} d^{-1}). Productivity transients were applied as a boxcar step change corresponding with the changes in environmental forcing (Table 1). The results represented by the red lines correspond with the results presented in Fig. 2c in the main text. Panels (b) and (c) demonstrate that the N_2' approach is equally skillful in representing excess ΔN_2 with both high and low rates of biological O_2 production, and that ΔN_2' is insensitive to ΔO_2.

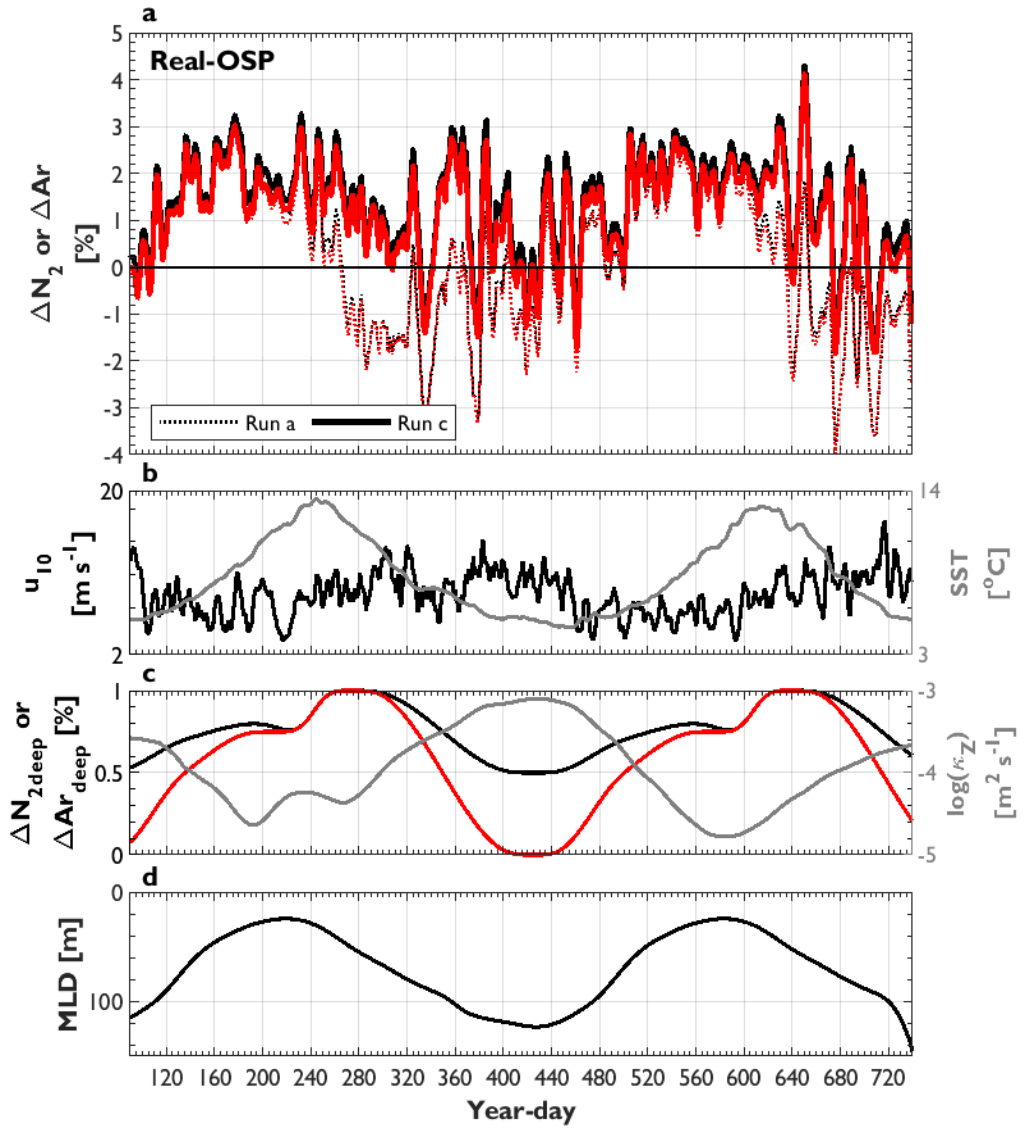

Figure S4. ΔN_2 (black) and ΔAr (red) in the realistic OSP simulation, with corresponding forcing parameters. In panel (a), solid lines represent output from the full-mixing simulation (i.e. run c), and dotted lines represent output from simulations with no mixing (run a). In panel (c), the black line represents subsurface ΔN_2, while the red line represents subsurface ΔAr. The x-axes represent April 2011-Jan. 2013. Refer to Figs. 3, 4 and Table 1 in the main text for further details.

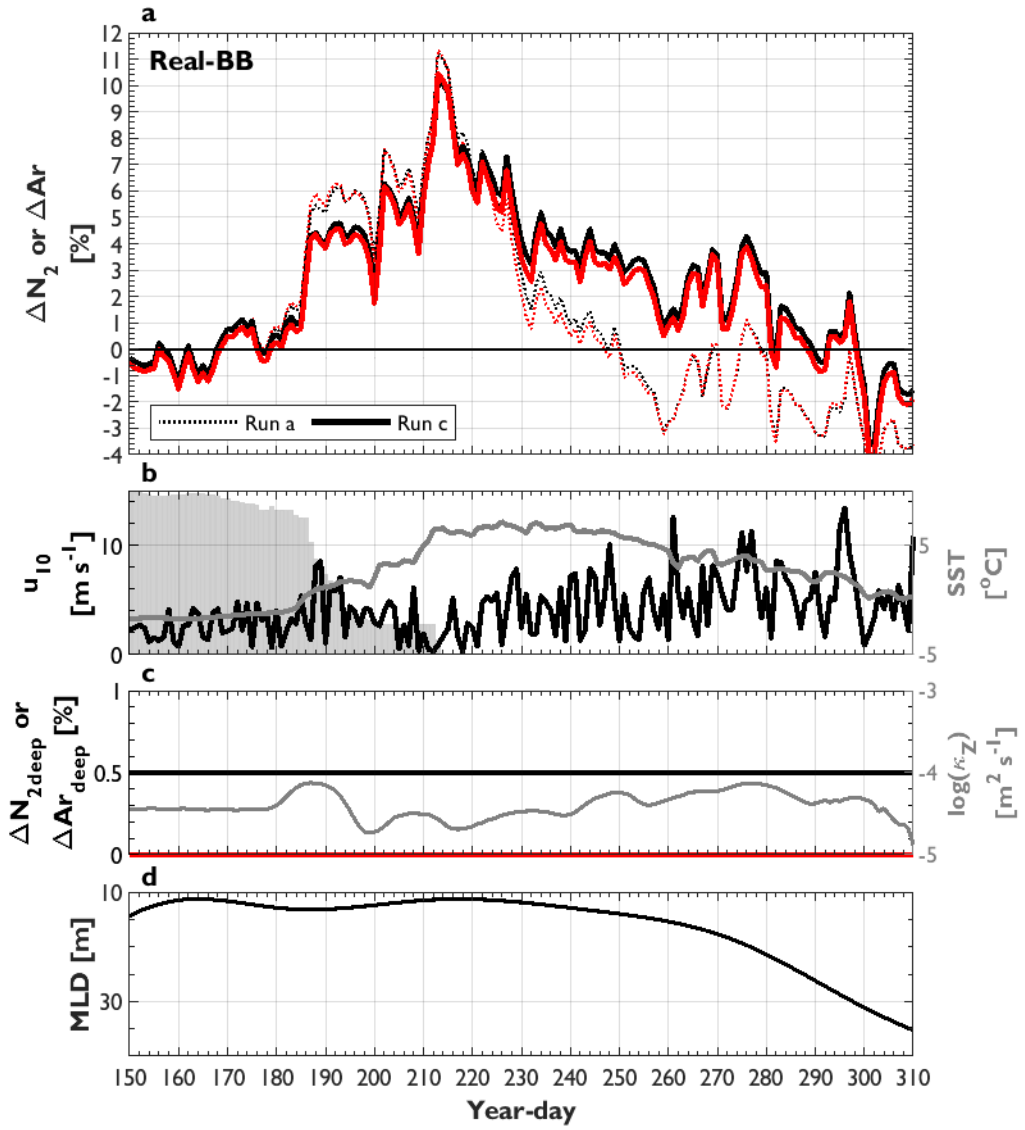

Figure S5. ΔN_2 (black) and ΔAr (red) in the realistic BB simulation, with corresponding forcing parameters. The x-axes represent 2019 year-day. Refer to Fig. S4 (above) and Figs. 3, 4 and Table 1 in the main text for further details.

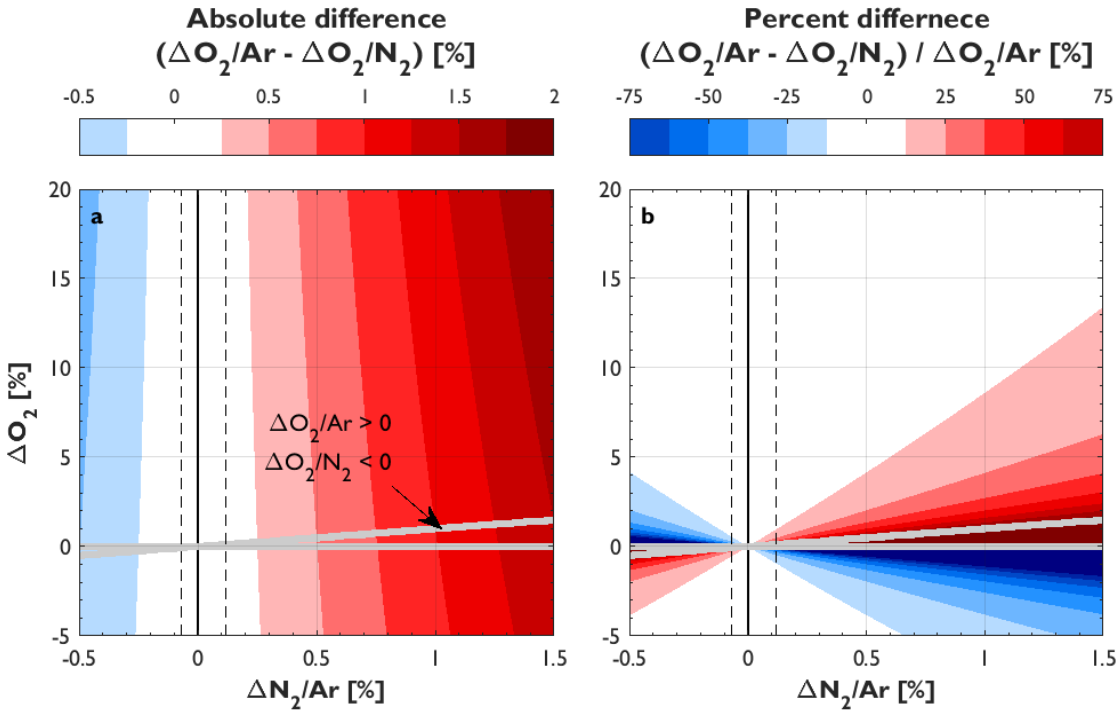

Figure S6. The absolute (a) and relative (b) differences between $\Delta O_2/Ar$ and $\Delta O_2/N_2$ over a realistic range of surface ΔO_2 in the ocean, and $\Delta N_2/Ar$ produced in the model simulations. Differences represent uncertainty in NCP estimates derived from O_2/N_2 if corrections for excess N_2 supersaturation are not made. The grey outlined region in both panels represents scenarios where $\Delta O_2/Ar$ and $\Delta O_2/N_2$ have opposite signs, leading to false interpretation of net tropic status from $\Delta O_2/N_2$. measurements. The vertical dashed lines represent the range of $\Delta N_2'/Ar$ (i.e. after correcting for excess N_2 supersaturation) in the realistic model simulations.

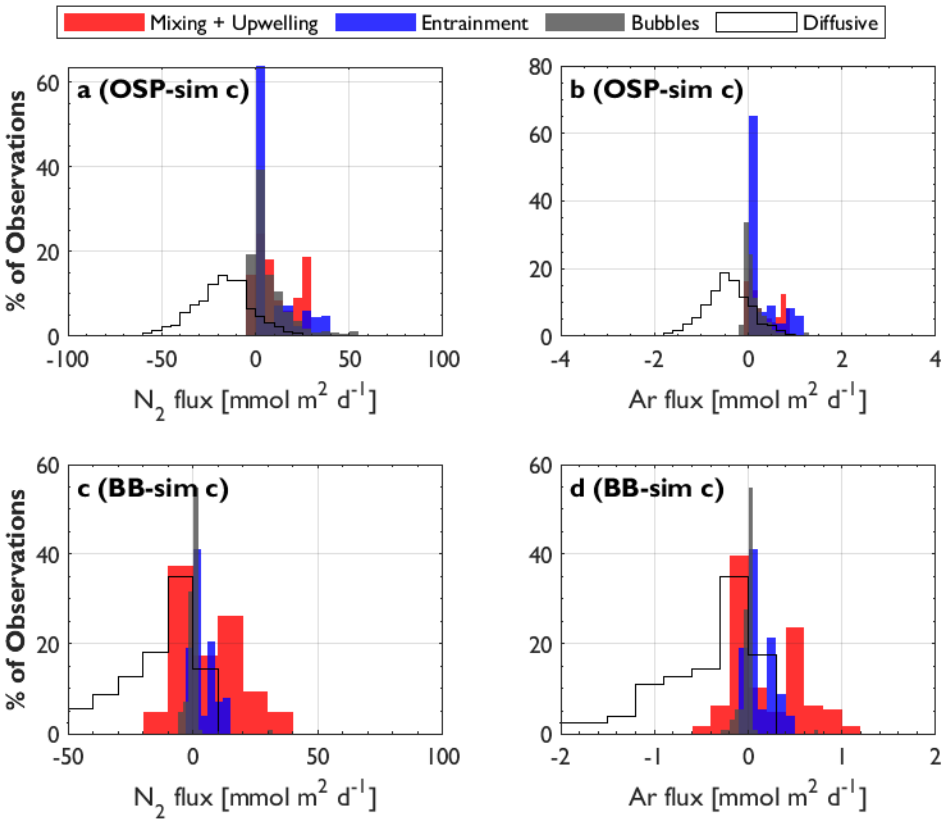

Figure S7. The frequency distribution of mixed layer fluxes in the realistic real-OSP (a, b) and real-BB (c, d) model run c (left = N_2; right = Ar). A positive flux represents an increase in the gas in the mixed layer.

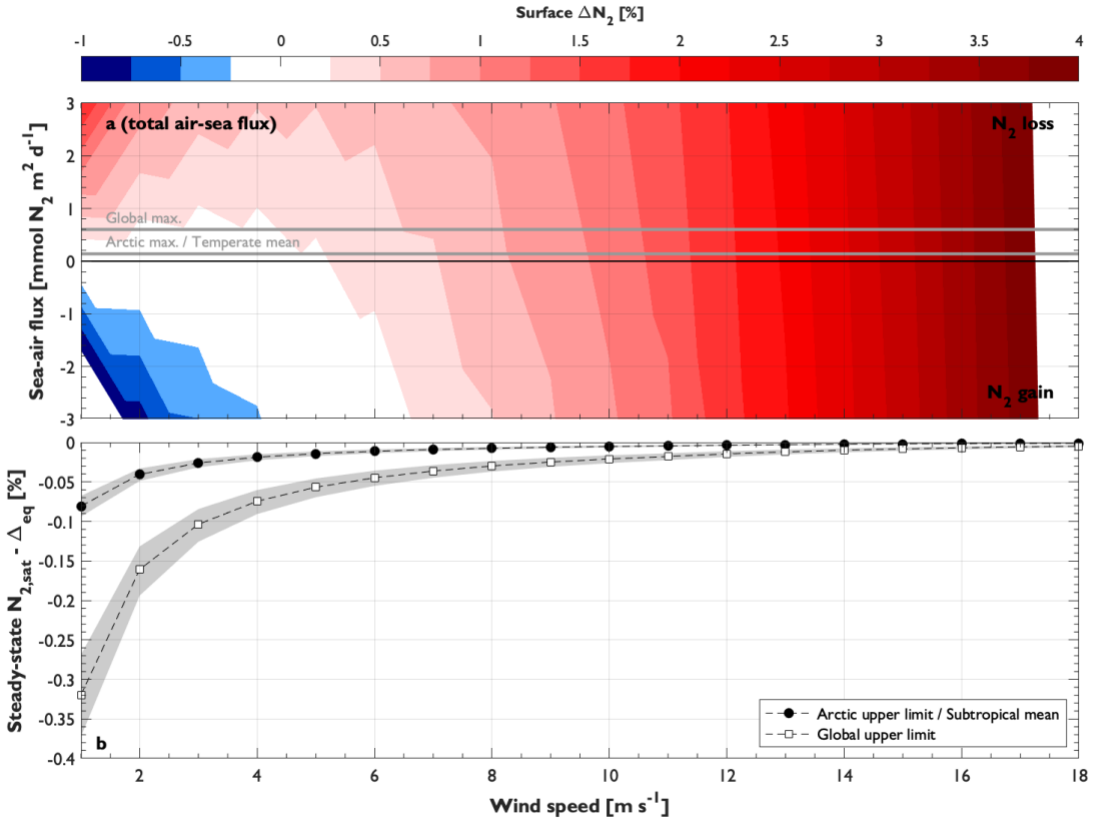

Figure S8. Relative importance of N_2 fixation and sea-air flux on surface N_2 supersaturation. Panel (a) shows the effect of total sea-to-air flux at various wind speeds, based on the Liang et al. (2013) exchange parameterization. Estimates of the global maximum and Arctic maximum / global subtropical mean N_2-fixation rates are shown as grey lines (details in main text), and the solid black line represents a N_2-fixation rate of zero. Biological N_2 removal is only significant when the magnitude of N_2-fixation exceeds the air-sea flux, which only occurs over a narrow range of conditions. Panel (b) shows the quasi-steady-state deviation of ΔN_2 from the bubble-induced supersaturation state ($\Delta_{eq,N2}$; Liang et al., 2013) for various wind speeds. Lines depict results calculated using different estimates of N_2-fixation rates, and shading represents the range of results over a range of temperate (0-25 °C) and salinity (0-35 PSU). A steady-state deviation value of 0 % means that bubble-mediated air-sea flux processes dominate over N_2-fixation. Other physical processes, including vertical mixing are ignored here. The x-scales on both panels are truncated at 18 m s^{-1} because air-sea fluxes almost always exceed N_2-fixation rates above this threshold.

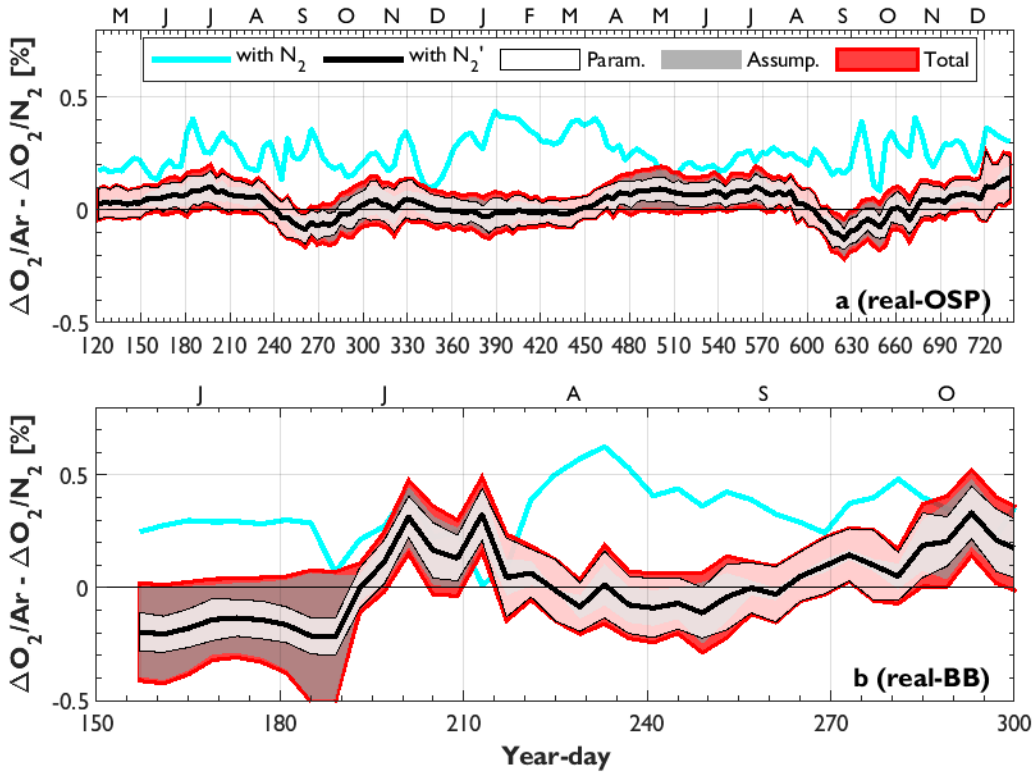

Figure S9. $\Delta O_2/Ar - \Delta O_2/N_2$ in the real-OSP (a) and real-BB (b) run c (full mixing) simulations. Uncertainty in $\Delta O_2/N_2$' is represented as shaded regions around model-derived $\Delta O_2/Ar - \Delta O_2/N_2$' values (black lines represent values with N_2', and blue lines are values with uncorrected N_2). The light grey patch represents the combined parameterization uncertainty, the dark grey patch is uncertainty from N_2' assumptions, and the red patch is the estimated total uncertainty, including the upper range of potential N_2-fixation. Mean uncertainty estimates are summarized in table S1.

Table S1. Sources of uncertainty in $\Delta O_2/N_2$', based on the full mixing runs of the realistic simulations (real-OSP run c, and real-BB run c). We performed Monte Carlo simulations by randomly applying parameter errors to each variable separately and in combination. Reported uncertainty (upper section, right column; in order of descending importance) represents the range and mean (in parentheses) of values across the model simulations. The error associated with the N_2' budget assumptions (i.e. constant salinity, MLD, κ, and $\Delta N_2/Ar_{deep}$) was evaluated by running an additional simulation in which these terms were set to the true values from the full 1D simulation environment. The total uncertainty presented at the bottom of the upper section was derived by summing in quadrature each of the underlined errors. Additional biases and uncertainty in NCP calculations are shown in the lower section of the table. NCP errors are based on Eq. 5 in the main text, over a realistic SST, salinity and u_{10} range.

Parameter	**Parameter Error**	**Absolute $\Delta O_2/N_2$' uncertainty [%]** Range (mean)
Sea surface temperature, SST	0.75 °C	0.02 – 0.1 (0.07)
Mixing coefficient, κ	10^{-5} m^2 s^{-1}	0.001 – 0.05 (0.02)
Wind speed, u_{10}	2.5 m s^{-1}	0.002 – 0.06 (0.01)
Bubbled flux scaling coefficient, β	0.14	<0.001 – 0.05 (0.01)
Diffusive air-sea flux, F_d	15 % (relative)	0.001 – 0.03 (0.008)
Mixed layer depth, MLD	5 m	<0.001 – 0.03 (0.006)
Partial bubble flux, F_P	15 % (relative)	<0.001 – 0.02 (0.004)
Subsurface $\Delta N_2/Ar$, $\Delta N_2/Ar_{deep}$	0.25 %	0.001 – 0.02 (0.004)
Sea level pressure, SLP	2 mbar	<0.001 – 0.004 (0.002)
Small bubble flux, F_C	15 % (relative)	<0.001– 0.007 (0.002)
	Combined parameterization	<u>0.04 – 0.2 (0.09)</u>
	All assumptions	<u>0.001 – 0.3 (0.07)</u>
	Total	**0.04 – 0.3 (0.1)**
	Surface N_2-fixation	<0.05

Additional biases

Parameter	**Parameter value [%]** Range (mean)	**NCP error [mmol O_2 m^{-2} d^{-1}]**
N_2 validation	0.9	N/A
Ex $\Delta O_2/Ar$ – $\Delta O_2/N_2$	0 – 1.1 (0.4)	0 - 19 (<7)
Real $\Delta O_2/Ar$ – $\Delta O_2/N_2$	0 – 0.8 (0.3)	0 – 14 (<6)
Ex $\Delta O_2/Ar$ – $\Delta O_2/N_2$'	0 – 0.5 (0.01)	0 – 9 (<0.2)
Real $\Delta O_2/Ar$ – $\Delta O_2/N_2$'	0 – 0.4 (0.01)	0 – 7 (<0.02)
Offshore mixing	N/A	0 – 50 (Izett et al., 2018)
Nearshore mixing	N/A	60 – 190 (Izett et al., 2018)
Diel $\Delta O_2/Ar$ variability	N/A	0 – 26 (Wang et al., 2020)